Oncostatin M and Kit-Ligand control hematopoietic stem cell fate during zebrafish embryogenesis

Mahony, Chris B.; Pasche, Corentin; Bertrand, Julien Y.

DOI:
10.1016/j.stemcr.2018.04.016

Document Version
Publisher's PDF, also known as Version of record

Citation for published version (Harvard):
Mahony, CB, Pasche, C & Bertrand, JY 2018, 'Oncostatin M and Kit-Ligand control hematopoietic stem cell fate during zebrafish embryogenesis' Stem Cell Reports, vol. 10, no. 6, pp. 1920-1934.
https://doi.org/10.1016/j.stemcr.2018.04.016

Stem Cell Reports
Article

OPEN ACCESS

Oncostatin M and *Kit-Ligand* Control Hematopoietic Stem Cell Fate during Zebrafish Embryogenesis

Christopher B. Mahony,[1] Corentin Pasche,[1] and Julien Y. Bertrand[1,*]
[1]University of Geneva, Faculty of Medicine, Department of Pathology and Immunology, CMU, University of Geneva, 1 Rue Michel-Servet, Geneva 1211, Switzerland
*Correspondence: julien.bertrand@unige.ch
https://doi.org/10.1016/j.stemcr.2018.04.016

SUMMARY

Understanding the molecular pathways controlling hematopoietic stem cell specification and expansion is a necessary milestone to perform regenerative medicine. Here, we used the zebrafish model to study the role of the *ckit* signaling pathway in this process. We show the importance of *kitb/kitlgb* signaling in the specification and expansion of hematopoietic stem cells (HSCs), in the hemogenic endothelium and caudal hematopoietic tissue (CHT), respectively. Moreover, we identified the zebrafish ortholog of *Oncostatin M* (*osm*) in the zebrafish genome. We show that the *osm/osmr* pathway acts upstream of *kitb* during specification of the hemogenic endothelium, while both pathways act synergistically to expand HSCs in the CHT. Moreover, we found that *osm*, in addition to its role in promoting HSC proliferation, inhibits HSC commitment to the lymphoid fate. Altogether, our data identified two cytokines, *kitlgb* and *osm*, secreted by the vascular niche, that control HSCs during early embryonic development.

INTRODUCTION

Hematopoietic stem cells (HSCs) are multipotent progenitors that sustain blood production from embryonic development to adulthood. Currently, *ex vivo* HSC expansion and HSC generation from induced pluripotent stem cells are the limiting factors toward achieving personalized cell-based regenerative medicine, creating a need to fully understand the signaling pathways involved in these processes. Definitive hematopoiesis development is very conserved in vertebrates. In both zebrafish and mammals, after primitive hematopoiesis has emerged, definitive hematopoiesis occurs in two waves: first, transient erythro-myeloid precursors (EMPs) arise in the yolk sac and posterior blood island, from mice (Bertrand et al., 2005) and zebrafish (Bertrand et al., 2007), respectively. Then, HSCs are specified from the aortic hemogenic endothelium. In the mouse embryo, HSC specification occurs along the ventral aspect of large arteries, predominantly in the aorta-gonads-mesonephros (AGM) region (Boisset et al., 2010; Chen et al., 2009; Zovein et al., 2008) between embryonic (E) day 9.5 and 11.5. In the zebrafish, HSCs are born at 32–60 hr post fertilization (hpf), from the hemogenic endothelium located in the dorsal aorta (Bertrand et al., 2010; Kissa and Herbomel, 2010). As the embryo makes a limited number of HSCs, they migrate to a first niche that will allow their expansion. In mouse, this initial expansion occurs in the fetal liver (Ema and Nakauchi, 2000), whereas zebrafish HSCs colonize the caudal hematopoietic tissue (CHT) (Tamplin et al., 2015). In both models, HSCs interact with endothelial cells (ECs) that promote their proliferation (Khan et al., 2016; Tamplin et al., 2015). We, and others, have shown that this expansion depends on several cytokines produced by stromal cells and caudal ECs (cECs) (Mahony et al., 2016; Tamplin et al., 2015).

Many studies performed in the mouse model demonstrated the importance of the *cKit/KitL* pathway in HSC maintenance *in vivo*, or HSC expansion *ex vivo* (Ding et al., 2012; Oostendorp et al., 2008). However, little is known about the role of *Kit* signaling during the emergence of definitive hematopoiesis in the mouse embryo. In zebrafish, the role of *kit* in hematopoiesis still remains unclear. The zebrafish genome encodes two paralogs, *kita* and *kitb*, following genome duplication and possible sub-functionalization (Mellgren and Johnson, 2005). *Kita*, but not *kitb*, is important for pigmentation and melanocyte development (Hultman et al., 2007) and appears not to be required for hematopoiesis, as adult *sparse* mutants ($kita^{-/-}$) show normal adult hematopoiesis (Parichy et al., 1999). Similarly, there are two paralogs for the stem cell factor (*kit-ligand*): *kitlga* is important for melanocyte normal development and, interestingly, *kitlgb* is expressed in the posterior blood island at 24 hpf (Hultman et al., 2007), strongly suggesting a role for this gene in zebrafish hematopoiesis. Furthermore, we recently showed that *kitlgb* could rescue the loss of HSCs observed in *tfec* mutants (Mahony et al., 2016). *KITL* also plays a major role in the expansion of human HSCs *ex vivo* but always in conjunction with other cytokines. Current clinical protocols targeting human HSCs for gene therapies usually use a cytokine cocktail composed of *KITL*, *FLT3L*, and *TPO* (Cavazzana-Calvo et al., 2000; Petzer et al., 1996; Ribeil et al., 2017). However, other cytokines seem to be potent to expand HSCs, such as human Oncostatin M (*OSM*). Oostendorp and colleagues showed that *KITL* together with *OSM*, but not by itself, could promote the expansion of immature human cord-

blood HSPCs and improve repopulating activity in NOD/SCID mice (Oostendorp et al., 2008). *OSM* mediated these effects by downregulating the *KITL*-induced MAPK/ERK pathway to preserve high CD34 expression (Oostendorp et al., 2008). This was further corroborated by studies showing that AGM hematopoiesis was enhanced *in vitro* by media containing a mix of *KIT*, *OSM*, *LIF*, and *FGF* (Nishikawa et al., 2001).

OSM is a cytokine belonging to the IL-6 family and has pleiotropic actions in hematopoiesis, inflammation, and neural development (Mukouyama et al., 1998; Rose et al., 1994; Tanaka and Miyajima, 2003). *Osm* binds a heterodimer that combines the *OSM* receptor chain (*OSMR*) and the signaling gp130 chain, which induces the intracellular activation of the JAK/STAT and MAPK pathways (Dey et al., 2013). *OSM* is expressed in a range of hematopoietic tissues, including thymus, bone marrow (BM), and spleen, and plays a role in the maintenance of hematopoietic progenitors through cell and non-cell autonomous mechanisms (Sato et al., 2014; Tamura et al., 2002; Tanaka et al., 2003). BM transplantation studies have shown that BM from wild-type (WT) mice transplanted into *Osmr*-deficient mice results in reduced erythrocytic/megakaryocytic progenitors. The same effect is observed when BM from *Osmr*-deficient mice is transplanted into WT mice (Tanaka et al., 2003). In contrast, ectopic overexpression of *Osm* resulted in enhanced extra-medullary hematopoiesis and increased megakaryocyte and platelet production (Wallace et al., 1995). Moreover, *Osm*-deficient mice show a reduced thymus size as well as an accumulation of apoptotic thymocytes, suggesting that a fine balance of *Osm* signaling is required for correct thymocyte development (Esashi et al., 2009).

In this study, we show that *kitb/kitlgb*, but not *kita/kitlga*, is required for HSC specification, emergence, and expansion in the CHT. We also identified the zebrafish ortholog *osm*, and characterized the function of this cytokine in zebrafish hematopoiesis. By combining different approaches, we show that zebrafish *osm* retains similar function to its mammalian ortholog and can expand HSCs, but also inhibits lymphoid commitment. We also show that interfering with *osmr* results in an early block in the specification of the hemogenic endothelium. Finally, we show that *osm* and *kitlgb* synergistically enhance HSC proliferation and decrease HSC differentiation.

RESULTS

Kitb, but Not *kita*, Signaling Is Necessary for HSC Specification

To understand the roles of *kita* and *kitb* in zebrafish HSC biology, we examined their expression during definitive hematopoiesis. In fluorescence-activated cell sorting (FACS)-sorted hematopoietic progenitors (EMPs and HSCs), we found that *kita* was mildly enriched in HSCs but found a much higher enrichment of *kitb* in both EMPs and HSCs (Figure 1A), although HSC enrichment was not significant compared with the whole embryo (Figure 1A). To further study these signaling pathways, we injected full-length mRNA for *kitlga* or *kitlgb* and knocked down the expression of *kita* and *kitb* using morpholinos (Figures S1A–S1D). The injection of *kitlga* and *kitlgb* mRNA did not alter *cmyb* expression at 4 days post fertilization (dpf) (Figure 1B). However, *kitb* morphants showed reduced *cmyb* expression at 4 dpf (Figure 1B) and reduced *rag1* expression at 4.5 dpf (Figure S1G). This loss of *cmyb* signal (i.e., loss of HSPCs in the CHT) likely resulted from a defect in HSC specification in *kitb* morphants, as shown by reduced levels of *runx1* and *cmyb* along the aorta at 28 and 36 hpf, respectively (Figure 1C). However, *gata2b* expression at 22 hpf was maintained in *kitb* morphants, indicating that specification of the hemogenic endothelium is not dependent on *kitb* signaling (Figure 1C). In contrast, the expression of *gata2b* at 22 hpf, *runx1* at 28 hpf, and *cmyb* at 36 hpf was normal in *kita* morphants (Figure 1C). The hematopoietic phenotype observed in *kitb* morphants was identical in *kiltgb* morphants (Figures 1D, S1E, and S1F). Both *kita* and *kitb* morphants displayed normal primitive myelopoiesis as detected by *mfap4* (primitive macrophages) and *mpx* (primitive neutrophils) expression (Figure S1H). Some *kitb* morphants had a modest reduction in primitive erythrocytes (Figure S1H) and some showed disrupted vasculature development (n = 5/12, data not shown). We also confirmed that *kitlga* mRNA injection resulted in hyper-pigmentation, while *kita* morphants had a reduction in the number of melanocytes over the yolk ball (Figures S1I–S1K), in agreement with previous studies (Hultman et al., 2007). In contrast, embryos injected with either *kitlgb* mRNA or the *kitb* morpholino showed no alteration of their pigmentation pattern (Figures S1I–S1K). We therefore conclude that *kita/kitlga* signaling is not required for definitive hematopoiesis but only for melanocyte development as previously suggested. We also conclude that *kitb/kitlgb* signaling is required for proper HSC specification, likely at the cell autonomous level, but one cannot exclude a non-cell autonomous mechanism, as a consequence of our qPCR data. Moreover, *kitlgb* gain of function by itself cannot increase HSC expansion, as we previously observed (Mahony et al., 2016). Therefore, we looked for a cytokine that could interact with *kitlgb* to promote HSC expansion.

Identification of Zebrafish *osm*

Based on previous human studies, we wanted to investigate the synergy between *osm* and *kitlgb* (Oostendorp et al.,

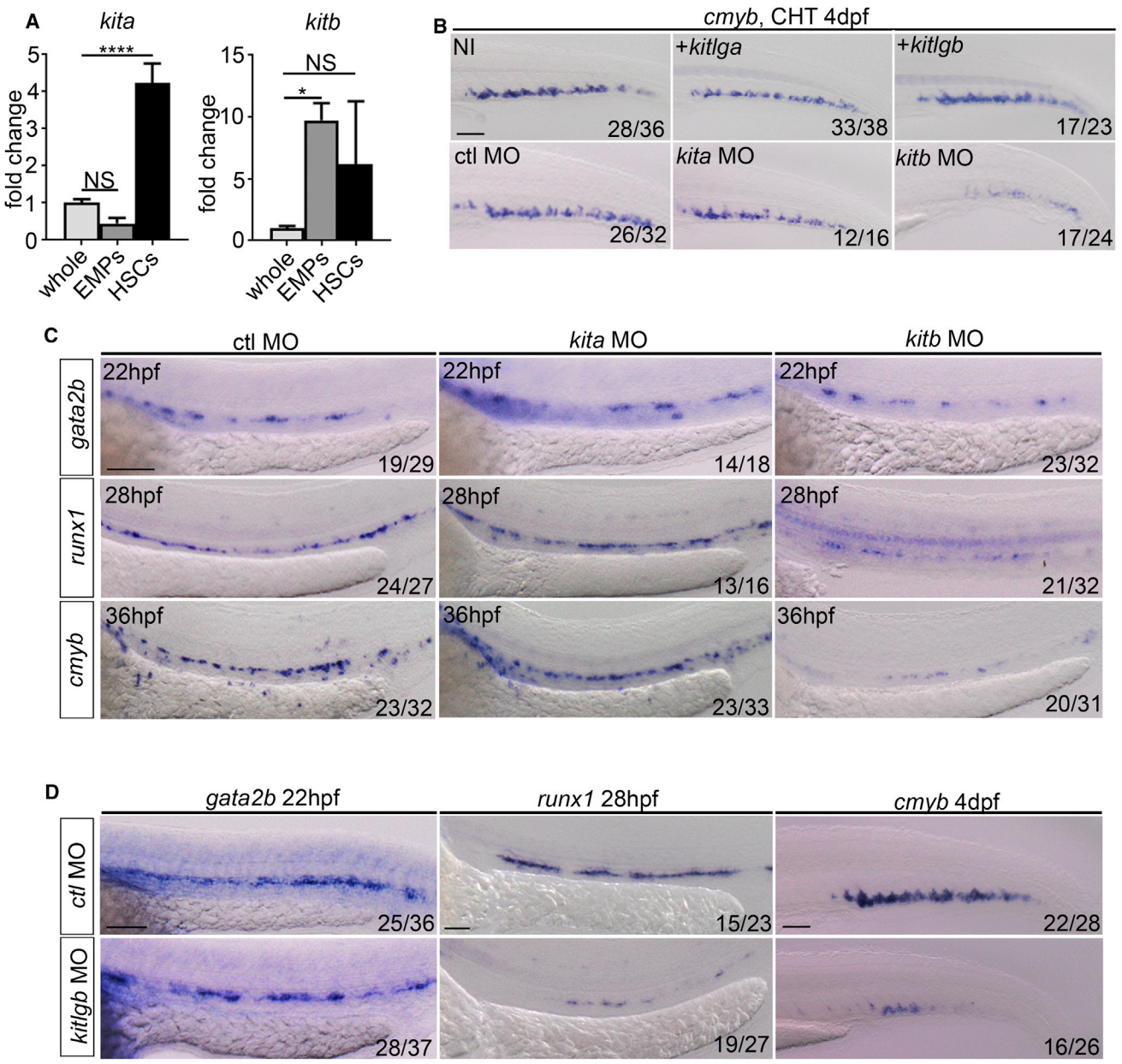

Figure 1. *kitb*, but Not *kita*, Signaling Is Necessary for Correct HSC Specification

(A) qPCR expression of *kita* and *kitb* in FACS-sorted hematopoietic progenitors. *Kita* whole and EMPS, p = 0.14. *kita* whole and HSCs, p < 0.0001. *kitb* whole and EMPs, p = 0.023. *kitb* whole and HSCs, p = 0.14. EMPs: double-positive *lmo2:eGFP*, *gata1:DsRed* cells (28 hpf) (Bertrand et al., 2007). HSCs: double-positive *flk1:mCherry*, *cmyb:eGFP* cells (36 hpf) (Bertrand et al., 2010). Data are from biological triplicates. Data are means ± SD.

(B) *cmyb* ISH at 4dpf in non-injected control (NI), *kitlga* (injected at 500 pg throughout, unless stated) or *kitlgb* (injected at 200 pg throughout, unless stated) mRNA injected embryos. *cmyb* was socred at 4dpf following ctrl-MO, *kita*-MO (injectedat 3 ng throughout, unless stated) or *kitb*-MO (injected at 8 ng throughout, unless stated) injection. NI, non-injected control. +*kitlga/kitlgb*, *kitlga/kitlgb* full length mRNA injected embryos.

(C) Control-MO, *kita*-MO and *kitb*-MO injected embryos were scored for the expression of *gata2b, runx1* and *cmyb* at 22 hpf, 28 hpf and 36 hpf, respectively. (D) *kitlgb* morphants were scored for *gata2b, runx1* and *cmyb* at 22 hpf, 28 hpf and 4 dpf, respectively. Analysis was completed using ordinary one way ANOVA with multiple comparisons. **** p < 0.0001; *p < 0.05; NS, p > 0.05. All scale bars, 100 μm.

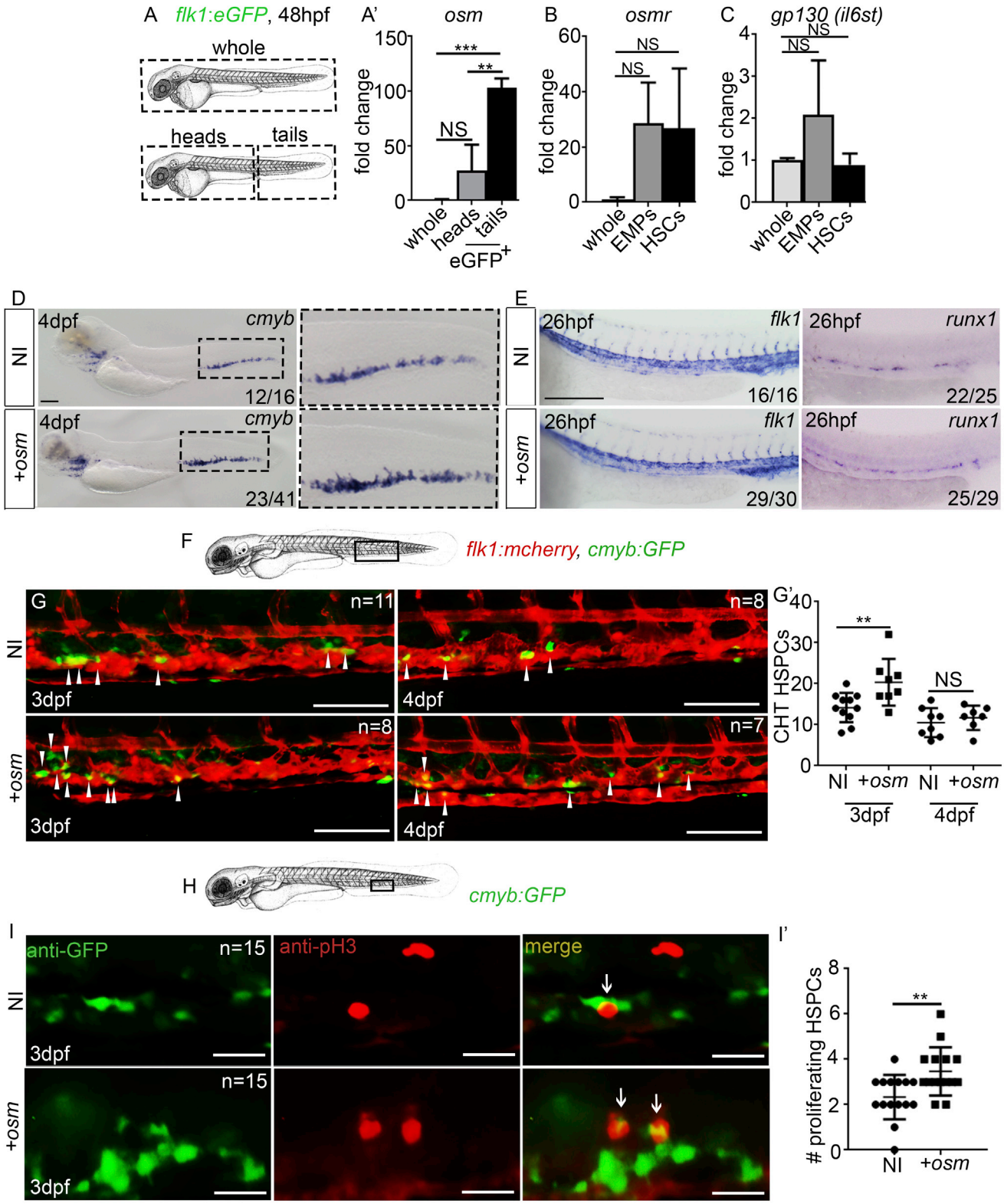

Figure 2. *osm* Expands HSCs within the CHT Niche

(A and A′) Experimental outline and qPCR expression of *osm* from whole zebrafish or FACS-sorted ECs. Data are biological triplicates plated in technical duplicates.

(legend continued on next page)

2008). However, no ortholog was annotated in the zebrafish genome. To identify *osm*, we proceeded by synteny analysis. The mouse and human *OSM* orthologs both lie in close proximity to *Gatsl* and *GATSL3*, respectively. In the zebrafish genome, we found a homologous transcript lying in close proximity to *gatsl3* (Figure S2A). This gene, annotated *si:ch73-47f2.1*, encodes a protein that segregates with the mouse and human *OSM* by phylogeny analysis but not with the other cytokines tested (Figure S2B). Furthermore, when we compared the gene structures of human *OSM*, mouse *Osm*, and zebrafish *si:ch73-47f2.1*, we found a similar arrangement consisting of three exons (Figure S2C). Amino acid similarity was low (26.3% with mouse *Osm*, 24.7% with human *OSM*, using EMBOSS Needle), but this has been previously noted in the characterization of other zebrafish cytokines when compared with their mammalian orthologs, such as *epo*, which shows 32% identity and 50% similarity between zebrafish and humans (Chu et al., 2007). Finally, *si:ch73-47f2.1* encodes a protein that contains a four-helical cytokine-like domain that is highly conserved with the mouse and human proteins (Figure S2D). We therefore conclude that *si:ch73-47f2.1* could be the zebrafish ortholog of the mammalian *OSM*. To further explore this hypothesis we examined the expression of *si:ch73-47f2.1/osm* and its receptor (*osmr*) and then examined their function during HSC ontogeny.

As the expression of *osm* was not detectable by *in situ* hybridization (ISH) (data not shown), we isolated cECs by FACS and performed qPCR. We found an enrichment of *osm* in the CHT vasculature compared with vasculature sorted from the rest of the embryo (Figures 2A and A′). Furthermore, *osmr* seemed highly enriched in definitive hematopoietic progenitors, EMPs and HSCs, compared with the whole embryo even if statistical significance was not reached (Figure 2B). In contrast, *gp130* was expressed rather ubiquitously (Figure 2C). Therefore, in zebrafish, as in mammals, the expression of *osm* and its receptor strongly correlates with a role in hematopoiesis. We next investigated the roles of this pathway in zebrafish HSCs.

osm Signaling Is Sufficient to Expand HSCs

Previous studies have reported that human *OSM* is capable of expanding human HSCs while inhibiting lymphoid differentiation (Kinoshita et al., 2001; Oostendorp et al., 2008). When we overexpressed *osm* by mRNA injection, we found a consistent increase in *cmyb* expression in the CHT compared with non-injected controls at 4 dpf (Figure 2D). *osm* mRNA injection did not change *runx1* or *flk1* expression at 26 hpf, and therefore did not increase HSC specification (Figure 2E). We then focused on HSCs within the niche using *flk1:mCherry;cmyb:eGFP* double transgenic embryos (Mahony et al., 2016; Tamplin et al., 2015) and found an increase in the number of HSCs within the niche at 3 dpf after *osm* gain of function compared with non-injected control embryos (Figures 2F–2G′). By 4 dpf, this increase was minimal and was close to control levels (Figures 2F–2G′). We then used *cmyb:GFP* embryos and stained for GFP and phospho-histone 3 (pH3), a marker of cell division, by immunofluorescence. Embryos injected with *osm* mRNA exhibited a significant increase in the number of proliferating HSCs within the CHT at 3 dpf (Figure 2H–2I′). Therefore, we conclude that the *osm* signaling pathway expands HSCs within the CHT by augmenting their proliferation, a result that was very similar to our previous work where we overexpressed *tfec* mRNA (Mahony et al., 2016). Accordingly, we found that *osm* expression was augmented in cECs after *tfec* overexpression (Figure S3A). Furthermore, *osm* overexpression could rescue the loss of *cmyb* expression observed in *tfec* mutants (Figures S3B and S3B′), supporting our conclusion that *osm* plays a role in expanding HSCs within the niche. We next examined the effect of *osm* on HSC differentiation.

osm Inhibits Lymphocyte Differentiation by Reducing Lymphoid Gene Expression

Previous studies showed that *OSM* suppresses commitment to the lymphoid fate (Kinoshita et al., 2001). We observed that *osm* mRNA injection decreased the thymus size at 4.5 dpf, indicating a decrease in HSC differentiation to

(B and C) qPCR expression of *osm*, *osmr*, and *gp130* (*il6st* in zebrafish) in whole zebrafish or FACS-sorted hematopoietic progenitors (EMPs and HSCs). All qPCR data are from biological triplicates. In (A′), (B), and (C), analysis was performed by a one-way ANOVA with multiple comparisons. In (A′), whole and heads, $p = 0.16$; whole and tails, $p = 0.0004$; heads and tails, $p = 0.0019$. In (B), whole and EMPs, $p = 0.17$; whole and HSCs, $p = 0.14$. In (C), whole and EMPs, $p = 0.22$; whole and HSCs, $p = 0.98$.

(D and E) ISH expression of *cmyb*, *flk1*, and *runx1* following injection of full-length *osm* mRNA (injected at 300 pg here and throughout, unless otherwise stated) or in non-injected embryos. Scale bar, 100 μm.

(F) Imaging area.

(G and G′) Imaging double transgenic *flk1:mCherry/cmyb:GFP* embryos at 3 and 4 dpf. Arrowheads represent HSCs embedded in the CHT niche. Scale bar, 100 μm. In (G′), between NI and *osm* injected at 3 dpf, $p = 0.0097$, and at 4 dpf, $p = 0.4894$.

(H) Imaging area.

(I and I′) anti-GFP and pH3 immunofluorescence at 3 dpf in *cmyb:eGFP* embryos. Arrows represent double-positive, proliferating cells. Scale bar, 25 μm. Analysis was performed by an unpaired, two-tailed Student's t test in (G′) and (I′). In (I′), $p = 0.0050$. NI, non-injected control. *+osm*, *osm* full-length mRNA-injected embryos. All data are means ± SD ***$p < 0.001$, **$p < 0.01$, NS, $p > 0.05$.

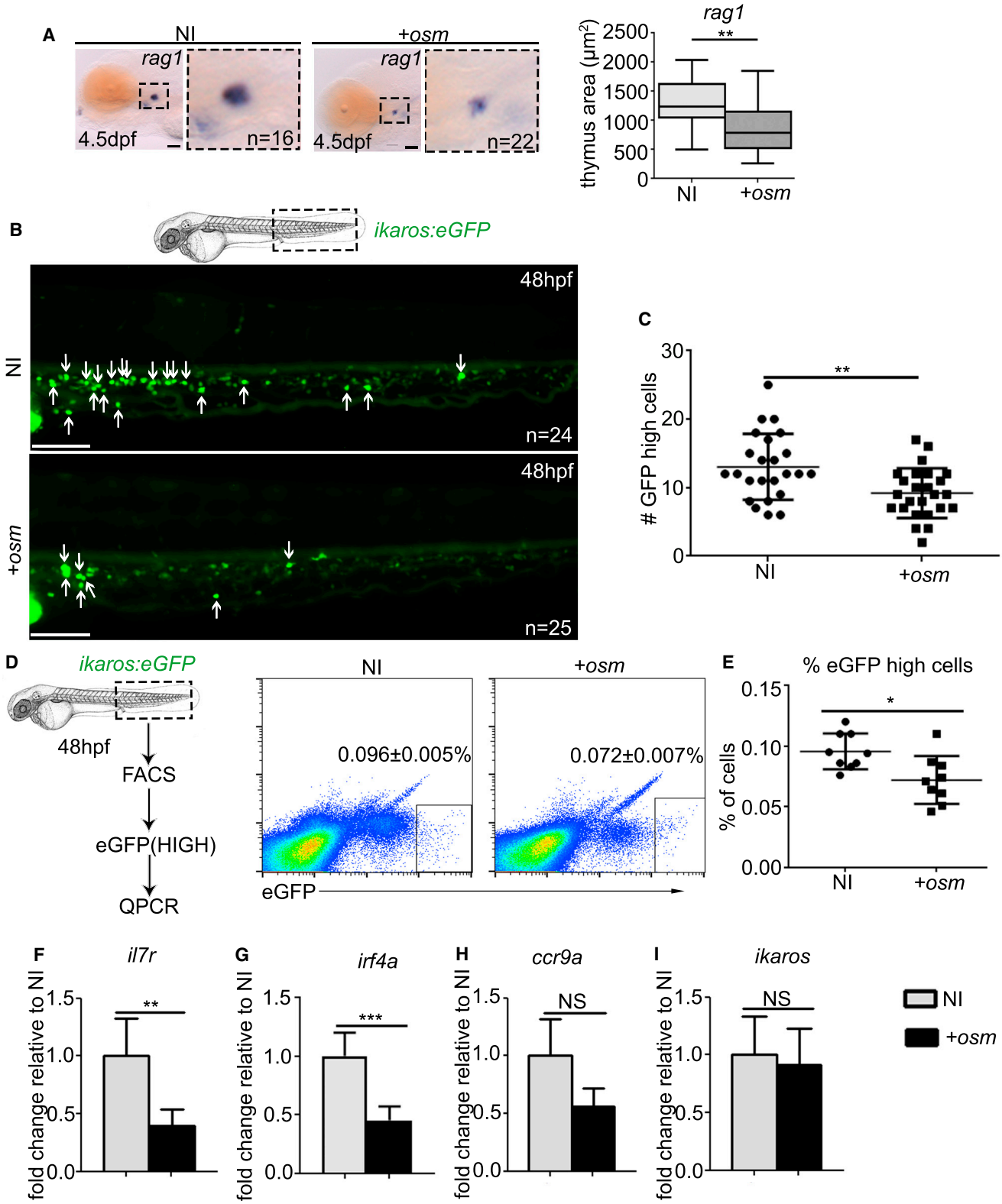

(legend on next page)

the T cell lineage (Figure 3A). To further examine this, we took advantage of the *ikaros:eGFP* transgenic line that marks lymphoid precursors (Hess and Boehm, 2012). First, we found a decreased number of lymphoid progenitors in the thymus in *osm*-injected embryos at 4.5 dpf (Figure S4A), suggesting a defect in thymic colonization. To understand this decrease, we examined the CHT of embryos at 48 hpf when lymphoid precursors are just beginning to seed the thymus (Murayama et al., 2006). At this stage, there is a distinct GFP^{high} population and many, more difficult to define GFP^{low} cells within the CHT. Injection of *osm* mRNA resulted in a severe decrease in the number of GFP^{high} cells at 48 hpf in the CHT (Figures 3B and 3C) probably resulting in the defect of thymic colonization observed at 4.5 dpf (Figure S4A). To further characterize the *ikaros:GFP^{high}* and *GFP^{low}* populations, we sorted these subsets from isolated tails dissected from control *ikaros:eGFP* embryos. We then investigated their gene expression pattern by qPCR (Figures S4B). *Ikaros*-GFP^{high} cells expressed high levels of *gata3*, *cmyb*, *ccr9a*, and *irf4a*. We therefore defined these cells as lymphoid-primed or lymphoid-committed HSCs (Figures S4C–S4P), according to previous results showing that *irf4a* is required for lymphoid commitment (Wang et al., 2015). Interestingly, both populations expressed high levels of *kitb* and *osmr* (Figures S4O and S4P).

To understand the defect in thymic hematopoiesis, we FACS sorted GFP^{high} cells from non-injected or *osm* mRNA-injected *ikaros:eGFP* embryos and measured, by qPCR, the expression levels of lymphoid genes (Figure 3D). First, in embryos injected with *osm* mRNA, we found a decrease in the percentage of GFP^{high} cells suggesting that *osm* inhibits HSC differentiation toward the lymphoid lineage (Figure 3E), concordant with our microscopy observations (Figure 3B). Second, we saw a decrease in the expression of *il7r*, *ccr9a*, and *irf4a* (although the decrease in *ccr9a* was not significant) (Figures 3F–3I), three important transcripts for T lymphopoiesis, but no change in *gata3*, *cmyb*, or *runx1*, three genes normally expressed in HSCs (Figures S3C and S3D). Therefore, *osm* not only expands HSCs but also inhibits their differentiation toward the lymphoid lineage by reducing the expression of several lymphoid receptors and transcription factors necessary for migration to and maturation in the thymus. Of note, the decrease in the number of *ikaros^{high}* cells in the CHT (Figures 3B and 3C) might have an additional explanation as it is also possible that *osm* acts directly upon the lymphoid-committed T cell progenitors that arise directly from the hemogenic endothelium (Tian et al., 2017). However, *osm* overexpression did not alter definitive erythropoiesis and granulopoiesis (Figure S3E–S3G), but the number of macrophages was slightly reduced (Figure S3F) in the CHT. We next inhibited *osmr* signaling to fully define the role of this signaling pathway in zebrafish hematopoiesis.

osmr Signaling Is Necessary for Early HSC Specification

During mouse embryogenesis, *Osm* is important for HSC emergence and may act at the level of the hemogenic endothelium (Mukouyama et al., 1998). *Osm* is also required for adult erythrocyte and megakaryocyte differentiation (Tanaka et al., 2003). We targeted *osmr* signaling by morpholino injection (Figures S5A–S5D). Compared with control embryos, *osmr* morphants exhibited an almost complete loss of aortic *gata2b*, *runx1*, and *cmyb* at 22 hpf, 28 hpf, and 36 hpf, respectively (Figure 4A). As a consequence, *cmyb* expression was completely lost in the CHT at 4 dpf and *rag1* was either severely reduced or completely lost at 4.5 dpf (Figures 4B and 4C). *Flk1*, *flt4*, and *dlc* expression was, however, normal in the aorta in *osmr* morphants at 28 hpf, indicating normal vessel specification (Figure S6A). *Osmr* morphants also showed reduced red blood cell circulation at 48 hpf (n = 16/20, Video S2) compared with control morphants (n = 10/10, Video S1). This correlated with a small decrease in *gata1* expression (Figure S6B) and a large decrease in *o*-dianisidine staining at 48 hpf in *osmr* morphants (Figure S6C). Furthermore, double transgenic *flk1:eGFP;gata1:DsRed osmr* morphants showed abnormal tail vasculature and reduced circulating red

Figure 3. *osm* Inhibits Lymphocyte Priming and Differentiation by Repressing Lymphoid Gene Expression

(A) ISH at 4.5 dpf of *rag1* thymus staining with quantification of thymus area, where p = 0.0087. Scale, 50 μm.

(B) Live imaging of CHT region in *ikaros:eGFP* embryos at 48 hpf. Each arrow indicates a single *ikaros:eGFP^{high}* cell. Scale, 100 μm.

(C) Quantification of the number *of ikaros:eGFP^{high}* cells at 48 hpf, p = 0.0028.

(D) FACS sorting and analysis of *ikaros:eGFP^{high}* cells at 48 hpf (p = 0.0112). Values indicated on FACS plots are mean ± SEM, graphs are means ± SD.

(E) Quantification of *ikaros:eGFP^{high}* cells.

(F–I) qPCR analysis of *il7r* (F) (p = 0.0017), *irf4a* (G) (p = 0.0001), *ccr9a* (H) (p = 0.1265), and *ikaros* (I) (p = 0.8030) expression in *ikaros:eGFP^{high}* cells FACS sorted at 48 hpf. qPCR data shown are the mean ± SEM of three data points, calculated from three independent experiments. Each separate experiment was conducted in biological triplicates, then averaged to give a single value. NI, non-injected control. *+osm*, *osm* full-length mRNA-injected embryos. Statistical analysis was completed using an unpaired, two-tailed Student's t test. ***p < 0.001; **p < 0.01; *p < 0.05; NS, p > 0.05.

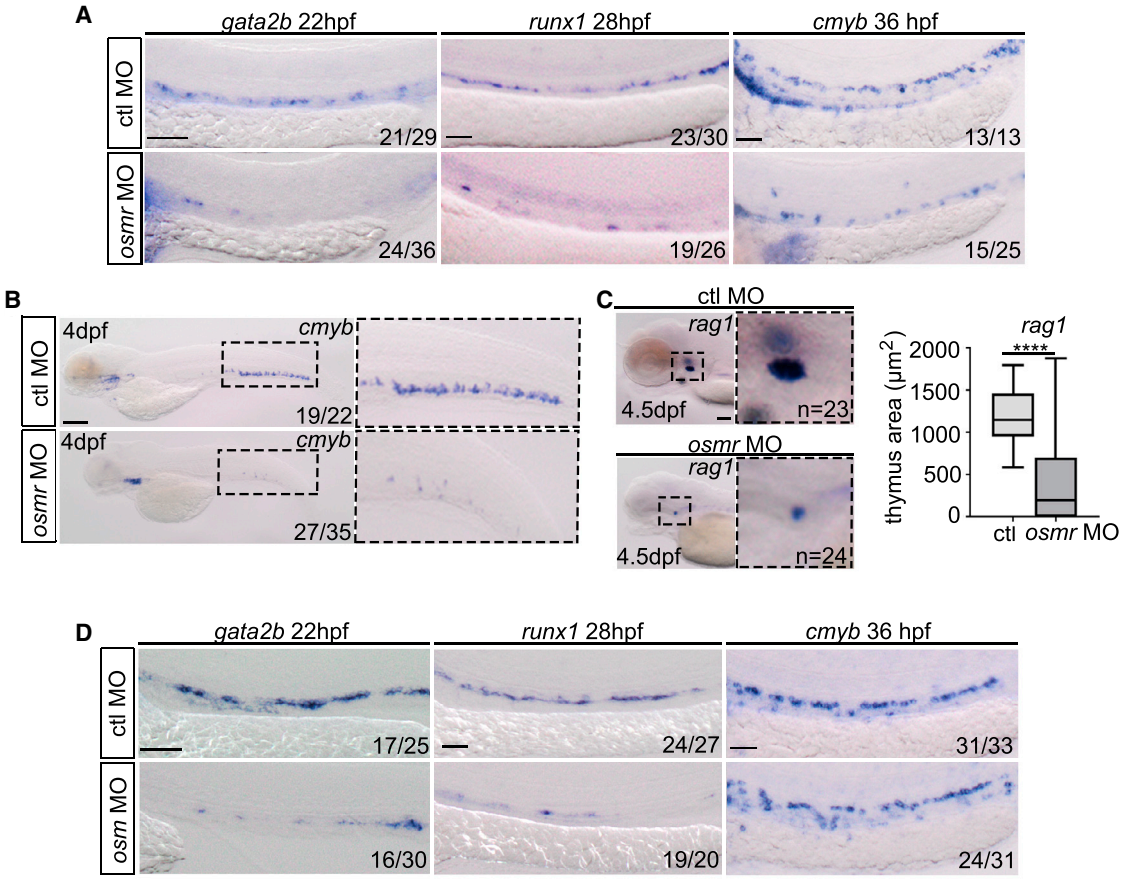

Figure 4. *osmr* Signaling Is Necessary for HSC Specification

(A) *gata2b*, *runx1*, and *cmyb* ISH in control MO, or *osmr* MO-injected embryos (injected at 4 ng throughout, unless stated). Scale bar, 100 μm. ctl, control.

(B) ISH expression of *cmyb*, in control MO, or *osmr* MO-injected embryos. Scale bar, 100 μm.

(C) *rag1* expression in the thymus after control MO or *osmr* MO injection, along with quantification of thymus area. Data are box and whiskers, min to max. Scale bar, 50 μm.

(D) *gata2b*, *runx1*, and *cmyb* ISH in control MO, or *osm* MO (injected at 7 ng throughout, unless stated)-injected embryos. Scale bar, 100 μm. Data are boxes and whiskers, min to max. Statistical analysis was completed using an unpaired, two-tailed Student's t test. ****$p < 0.0001$.

blood cells compared with control embryos at 48 hpf (Figure S6D). However, primitive myelopoiesis was completely normal (Figure S6E). We directly targeted *osm* expression by morpholino (Figures S5E and S5F) and recapitulated the hematopoietic phenotypes observed in *osmr* morphants (Figure 4D). However, we did observe that the majority of *osm* morphants display normal *cmyb* expression at 36 hpf, indicating a recover from the reduction of *gata2b/runx1* expression (Figure 4D). We conclude that *osm* overexpression is sufficient to expand HSCs and that *osmr* signaling is necessary for HSC specification and primitive erythropoiesis, but not for primitive myelopoiesis. We next examined the synergistic effects of *osm* and *kitlgb* on HSC expansion and HSC emergence.

osm and *kitlgb* Synergistically Expand HSCs and Increase HSC Proliferation

As we, and others, have found that *kita* plays a major role in pigmentation but not hematopoiesis (Hultman et al., 2007; Parichy et al., 1999), we investigated any possible synergy between the *kitlgb/kitb* and *osm/osmr* pathways. The injection of subliminal doses of *kitlgb* and *osm* mRNA alone resulted in no change in *runx1* (28 hpf) or *cmyb* (4 dpf) expression (Figures 5A–B′). However, injecting both mRNAs into the same embryo resulted in a strong increase of *cmyb* (4 dpf) in the CHT, although *runx1* was not affected at 28 hpf (Figures 5A–5B′), which likely resulted from increased HSC proliferation in the CHT, as measured by pH3 staining (Figures 5C–5D′). We therefore conclude

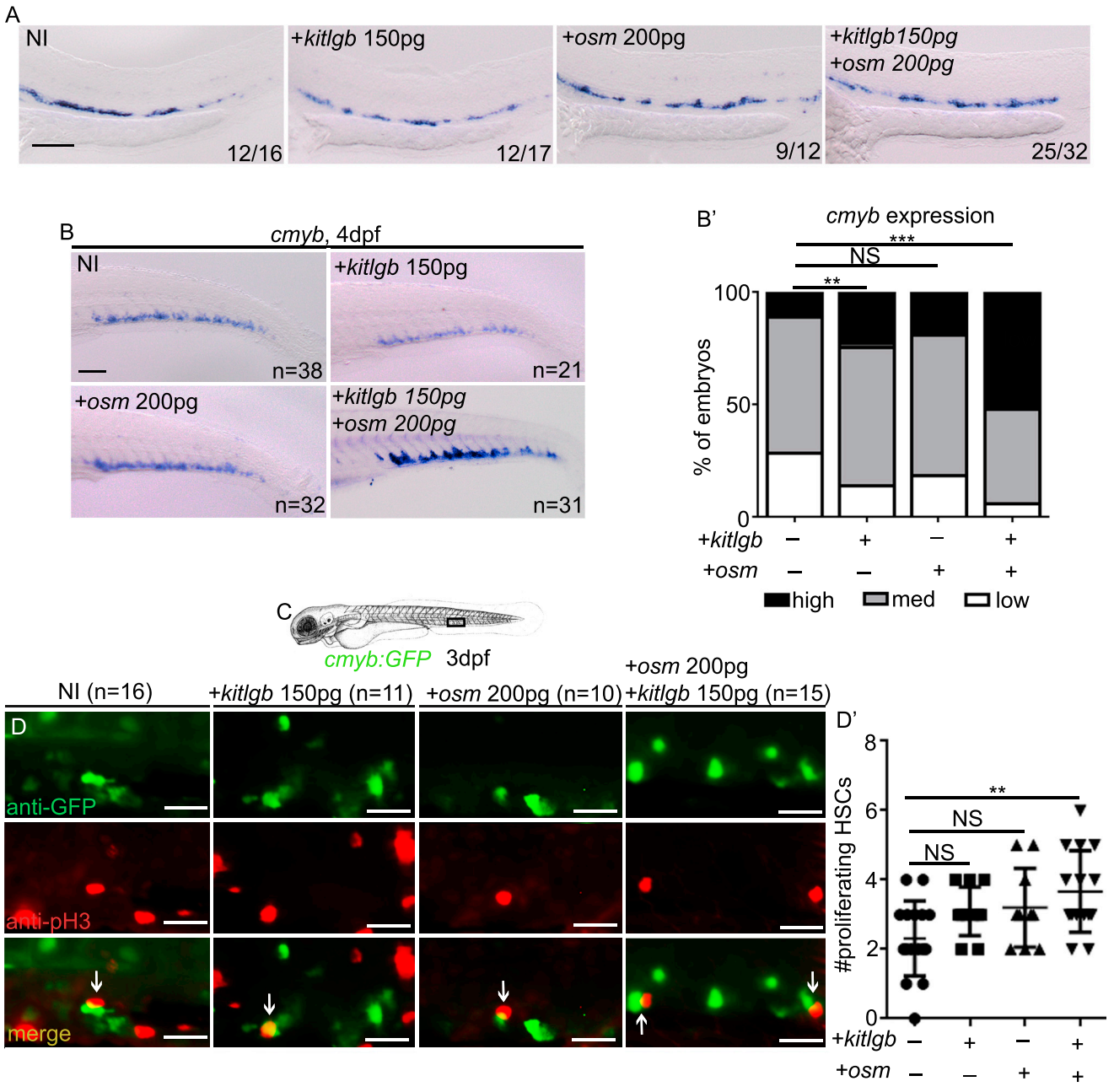

Figure 5. *osm* and *kitlgb* Signal Synergistically to Expand HSCs in the CHT

(A) *runx1* ISH at 28 hpf in NI embryos and *kitlgb* or *osm* mRNA-injected embryos (injected separately and together) at subliminal doses. Scale bar, 100 μm.

(B) *cmyb* ISH at 4 dpf in NI embryos and *kitlgb* or *osm* mRNA-injected embryos (injected separately and together) at subliminal doses. Scale bar, 100 μm.

(B′) *cmyb* expression analysis. Analysis is Fisher's exact test. NI versus *kitlgb*, p = 0.29; NI versus *osm*, p = 0.48; NI versus *kitlgb* + *osm*, p = 0.0001.

(C) Imaging schematic.

(D) Immunofluorescence for GFP and pH3. Arrows represent double-positive, proliferating cells. Scale, 25 μm.

(D′) Quantification of double-positive cells. (D′) Data are means ± SD and analysis is an ordinary one-way ANOVA with multiple comparisons. ANOVA p value = 0.0082. ***p < 0.001; **p < 0.01; NS, p > 0.05.

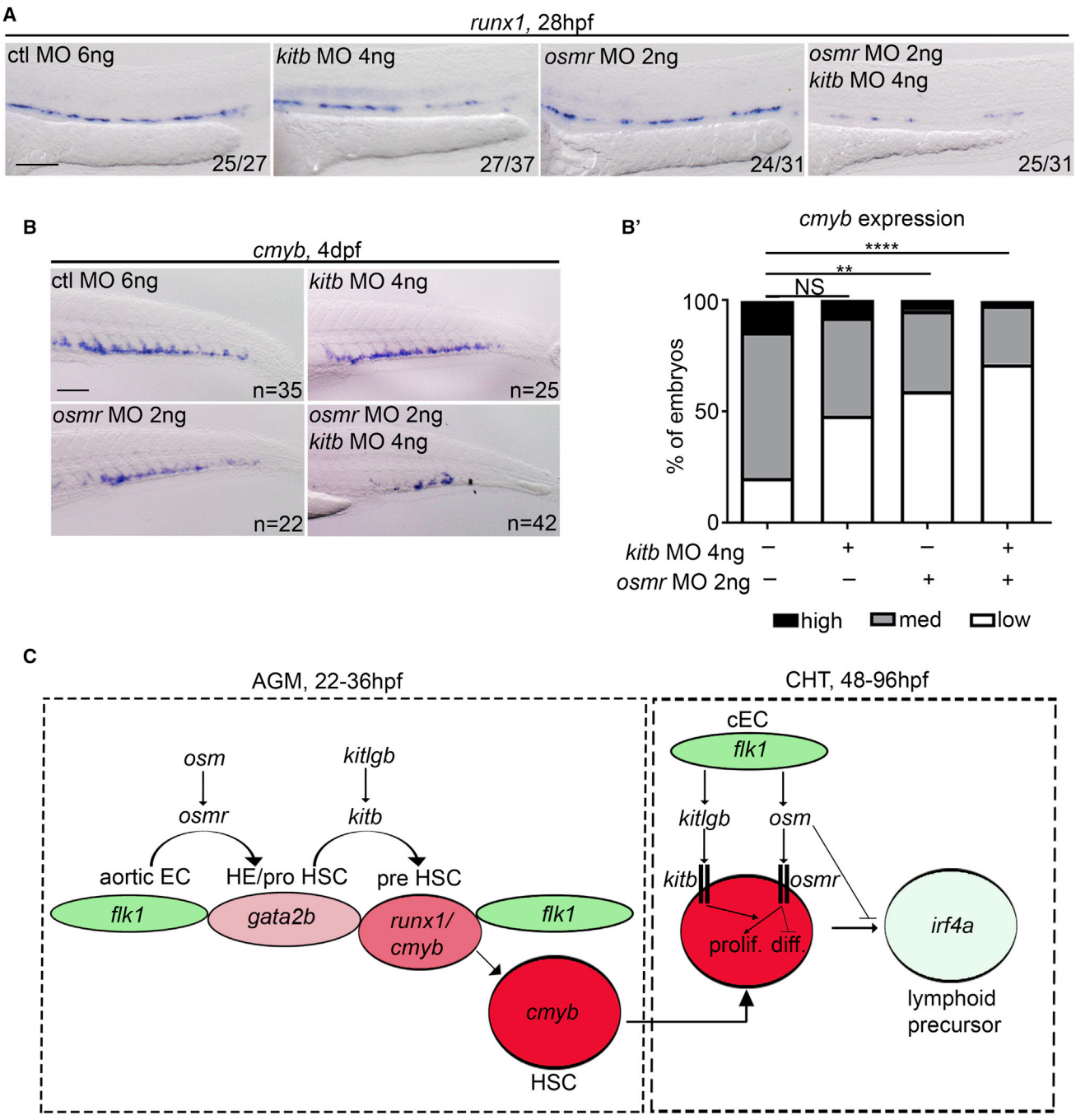

Figure 6. Inhibition of *osmr* and *kitb* Signaling Synergistically Inhibits HSC Specification

(A) *runx1* (28 hpf) ISH following control MO, *osmr* MO, or *kitb* MO injection (separately and together) at subliminal doses (half doses). ctl, control.

(B) *cmyb* ISH at 4 dpf following control MO, *osmr* MO, or *kitb* MO injection (separately and together) at subliminal doses (half doses). (B′) Quantification of the results observed in panel (B). High *cmyb*signal (black), medium *cmyb* signal (grey) and low *cmyb* signal (white). Analysis was generated by Fisher's exact test. NI versus *kitb-MO*; p = 0.082, NI versus *osmr-MO*; p = 0.0089, NI versus *kitb+osmr-MOs*; p = 0.0000009.

(C) Summary. Aortic ECs transition to "HE/pro HSC" by expressing *gata2b*, a process that requires *osm/osmr* signaling. HSCs then begin to bud from the aorta and begin to express *runx1* to become "pre HSCs", a process that requires *kitlgb/kitb* signaling. HSC then become "HSCs"

(legend continued on next page)

that these cytokines act synergistically to expand HSCs after they arrive in the CHT.

To further examine this synergistic effect, we co-injected morpholinos against *kitb* or *osmr*, at subliminal doses. Injections of each morpholino alone resulted in normal *runx1* at 28 hpf and *cmyb* expression at 4 dpf (Figure 6A–6B′). However, when injected together, a robust decrease in *runx1* at 28 hpf and *cmyb* at 4 dpf was observed (Figures 6A and 6B′). Altogether, these experiments show that both *kitb* and *osmr* signaling pathways act together to specify, and then expand, HSCs in the CHT (Figure 6C).

DISCUSSION

We have investigated *kit* signaling in zebrafish hematopoiesis and shown interesting functional differences between the *kit* and *kitlg* paralogs, despite their relative similarities. We found that *kita/kiltga* signaling is important for pigmentation but not for hematopoiesis, concordant with previous reports (Hultman et al., 2007; Parichy et al., 1999). Furthermore, *kita* is expressed in neural crests and *sparse* (*kita*) mutants survive, are healthy, and only have reduced melanocyte numbers (Parichy et al., 1999). We also showed that *kitlgb/kitb* signaling is required for zebrafish hematopoiesis. Our data indicate that *kitlgb* preferentially signals through *kitb*, while *kitlga* signals through *kita*, but we cannot exclude any cross-activation of these ligands with the two receptors, as low levels of *kita* were detected in HSCs. A previous report showed that *kitlgb* is expressed within the posterior blood island, the tissue that will give rise to the CHT at 24 hpf (Hultman et al., 2007). As EMPs are born in this area, we also checked their numbers in *kitb* morphants but could not find any difference at 30 hpf (data not shown). However, *kitb* but not *kita* morphants showed a strong decrease of *runx1* along the aorta. Work in the mouse embryo has indicated that *Kit-L* was required, not for the initial specification of the hemogenic endothelium into pro-HSCs, but rather for the maturation and maintenance of HSCs in mouse AGM cultures (Rybtsov et al., 2014). Further studies have shown that cells at the base of aortic HSC clusters are highly proliferative and express higher levels of *c-Kit* (Batsivari et al., 2017). As we found that *gata2b* is maintained, but *runx1* is lost, in *kitb* morphants, we conclude that, as in mammals, *kitb* signaling is not required for the initial specification of the hemogenic endothelium but rather for the maturation of pro-HSCs into *runx1/cmyb*-positive pre-HSCs, to follow the mouse nomenclature that has been proposed (Rybtsov et al., 2014). Moreover, *kitb* signaling seems to be also required for HSC expansion at later stages (Figure 6C).

However, as we previously described, the overexpression of *kitlgb* by itself cannot expand HSCs in the CHT (Mahony et al., 2016). Therefore, we started to investigate for potential cytokines that could act together with *kitlgb*. As mouse and human oncostatin M showed promising results (Nishikawa et al., 2001; Oostendorp et al., 2008), we undertook to find the ortholog of this cytokine in the zebrafish genome. Based on synteny and sequence similarities, we established that *si:ch73-47f2*.1 was the most likely candidate. Moreover, our data indicate that targeting *si:ch73-47f2*.1 by morpholino induces the exact same phenotypes observed in *osmr* morphants. Altogether, our data suggest that *si:ch73-47f2*.1 is the zebrafish ortholog of *Oncostatin M*. However, we were unable to find orthologs of *si:ch73-47f2*.1 in many other closely related fish species (such as *Sinocyclocheilus rhinocerous* and medaka), although in many cases an ortholog for *osmr* is listed. This, coupled with the low amino acid similarity, raises the possibility that *si:ch73-47f2*.1 could encode a novel, zebrafish-specific regulator of hematopoiesis that would be related to, but distinct from, *osm*. We show that *osm* is expressed in the CHT vascular niche under the control of *tfec*, a transcription factor that also controls *kitlgb* expression (Mahony et al., 2016). Indeed, *osm* could rescue the HSC defect observed in *tfec* mutants and, in contrast to *kitlgb*, *osm* could increase the number of HSCs in the CHT, but we did not observe any increase of HSCs in the aorta, as was observed for mouse AGM-HSCs (Mukouyama et al., 1998). In the CHT, *osm* acted by increasing HSC proliferation, similarly to *tfec* gain of function, and we observed that this HSC expansion was accompanied by a reduction of lymphoid development. Indeed, we show here that *osm* downregulates *irf4a*, a transcription factor required for lymphopoiesis that also controls *ccr9a* expression (Wang et al., 2015). Our results suggest that *osm* negatively regulates the expression of several lymphoid genes within lymphoid-primed progenitors. Our results corroborate a previous report showing that mouse *OSM* can inhibit the differentiation of HSCs toward the lymphoid lineage in the mouse fetal liver (Kinoshita et al., 2001). However, this study mainly focused on embryonic B cell lymphopoiesis (Kinoshita et al., 2001), whereas our results point to the effect of *osm* on T cell commitment. It is possible that *osm* mediates a similar effect upon B cell differentiation but, due to the late emergence of B lymphopoiesis in zebrafish (around 20 dpf) (Page et al., 2013), we could not test this

and express *cmyb*. HSCs migrate to the CHT and can either proliferate (prolif.) or differentiate (diff.) in response to cytokines expressed by caudal ECs (cECs). Some will differentiate to lymphoid lineages. Proliferation of HSCs is enhanced by *osm* and differentiation to lymphoid lineages is inhibited. HSC proliferation is also synergistically enhanced by both *kitlgb* and *osm* signaling through their receptors. ****$p < 0.0001$; **$p < 0.01$. All scale bars, 100 μm. HE, hemogenic endothelium.

hypothesis in our experiments. Furthermore, Esashi et al. (2009) described that *OSM* deficiency led to a decreased thymic size and the accumulation of apoptotic thymocytes in the adult mouse. Zebrafish *osm* may also be required for thymic maintenance in a similar manner, as we show that the deficiency in the *osm* pathway decreases definitive hematopoiesis, therefore resulting in a smaller thymus.

We indeed found that *osmr* signaling is necessary for early HSC specification, as indicated by the loss of *gata2b/runx1* in *osmr* morphants. This role of *osm* might have been conserved throughout evolution. Indeed, *Osm* is expressed in the mouse AGM region, in the genital ridges and the sub-aortic mesenchyme (Mukouyama et al., 1998). Moreover, *Osmr* is highly enriched in ECs and newly formed hematopoietic progenitors from the human AGM but downregulated in fetal liver hematopoietic progenitors (Ng et al., 2016). We therefore conclude that the *osm* signaling pathway is important for the emergence of HSCs (Figure 6C).

Finally, we tested a possible synergistic effect between both *osm/osmr* and *kitlgb/kitb* pathways, as it was previously demonstrated in the expansion of human HSCs (Oostendorp et al., 2008). We first showed that subliminal inhibition of both *osmr* and *kitb* receptors leads to a complete loss of HSC specification, whereas each morpholino on its own had no effect on HSC specification. As we show that the block induced in *osmr* morphants occurs at an earlier stage than the one induced by the *kitb* morpholino, we conclude that both signals are required sequentially for normal HSC specification. Concerning HSC expansion in the CHT, we have shown that *osm* and *kitlgb* overexpression is sufficient to expand hematopoiesis *in vivo*, which corroborates results gained from *in vitro* analysis on human HSCs (Oostendorp et al., 2008). Altogether, our data convincingly show that the *kit* pathway has been conserved in the zebrafish model to allow normal HSC development. Moreover, we show that it acts together with the *osm/osmr* pathway during HSC specification from the hemogenic endothelium and for the expansion phase in the CHT. Moreover, by modulating these two pathways, we could unravel discrete stages of HSC specification from the hemogenic endothelium. Further studies will be required to fully understand the precise sequence of events, as well as the source of the signals.

EXPERIMENTAL PROCEDURES

Zebrafish Strains and Husbandry

AB* (WT), along with transgenic and mutant strains, were kept in a 14/10 hr light/dark cycle at 28°C (Westerfield, 1994). We used the following transgenic animals: *lmo2:eGFP*^{zf71} (Zhu et al., 2005), *gata1:DsRed*^{sd2} (Traver et al., 2003), *flk1:eGFP*^{s843} (Jin et al., 2005), *flk1:Hsa.HRAS-mCherry*^{s896} (Chi et al., 2008), *cmyb:GFP*^{zf169} (North et al., 2007), *ikaros:eGFP*^{fr101} (Hess and Boehm, 2012), *tfec*^{ug103} mutants (Mahony et al., 2016).

Whole-Mount *In Situ* Hybridization Staining and Analysis

Whole-mount *in situ* hybridization (WISH) was performed on 4% paraformaldehyde (PFA)-fixed embryos at the developmental time points indicated. Digoxygenin labeled probes were synthesized using an RNA labeling kit (SP6/T7; Roche). RNA probes were generated by linearization of TOPO-TA or ZeroBlunt vectors (Invitrogen) containing the PCR-amplified cDNA sequence. WISH was performed as previously described (Thisse et al., 1993). Phenotypes were scored by comparing expression with siblings. All injections were repeated three independent times. Analysis was performed using GraphPad Prism software. Embryos were imaged in 100% glycerol using an Olympus MVX10 microscope. Oligonucleotide primers used for the production of ISH probes are listed in Table S1.

O-Dianisidine Staining

Embryos at 48 hpf were stained in 0.9 mg/mL o-dianisidine (Sigma), 10 mM sodium acetate (pH 4.5), 0.65% hydrogen peroxide, 60% ethanol for 25 min in the dark, and then fixed in 4% PFA for 1 hr at 4°C and imaged in 70% glycerol.

Cell Sorting and Flow Cytometry

Zebrafish transgenic embryos (15–20 per biological replicate) were incubated in 0.5 mg/mL Liberase (Roche) solution and shaken for 90 min at 33°C, then dissociated, filtered, and resuspended in 0.9× PBS and 1% FCS. Dead cells were labeled and excluded by staining with 5 nM SYTOX red (Life Technologies) or 300 nM DRAQ7 (Biostatus). Cell sorting was performed using an Aria II (BD Biosciences) or a Bio-Rad S3. Data were analyzed using FlowJo and statistical analysis completed using Microsoft Excel or GraphPad Prism.

Real-Time qPCR and qPCR Analysis

RNA was extracted using an RNeasy minikit (QIAGEN) and reverse transcribed into cDNA using a Superscript III kit (Invitrogen) or qScript (Quanta Biosciences). qPCR was performed using KAPA SYBR FAST Universal qPCR Kit (Kapa Biosystems) and run on a CFX Connect real-time system (Bio-Rad). All primers are listed in Table S2. Analysis was performed using Microsoft Excel or Prism.

Synthesis of Full-Length mRNA and Microinjection

PCR primers to amplify cDNA of interest are listed in Table S1. *Tfec* mRNA was synthesized and injected as previously described (Mahony et al., 2016). mRNA was reverse transcribed using mMessage mMachine kit SP6 (Ambion) from a linearized pCS2^{+} vector containing PCR products. Following transcription, RNA was purified by phenol-chloroform extraction. *osm* mRNA was injected at 300 pg, unless otherwise stated.

Imaging

WISH was imaged using an Olympus MVX10 microscope in 100% glycerol. Fluorescent images were taken with an Olympus IX83 microscope and processed using cellSens Dimension software. All images were processed using Adobe Photoshop.

Immunofluorescence Staining

Images were obtained with a Nikon SMZ1500 microscope or a Nikon inverted A1r spectral confocal microscope. Z stacks were made through the entire CHT during confocal imaging in multiple fluorescent channels. Immunofluorescence double staining was carried out and analyzed as described previously (Gao et al., 2015), with chicken anti-GFP (1:400, Life Technologies, catalog no. A10262) and rabbit anti-phospho-histone 3 (pH3) antibodies (1:250, abcam, catalog no. ab5176). AlexaFluor488-conjugated anti-chicken secondary antibody (1:1,000, Life Technologies, catalog no A11039) and AlexaFluor594-conjugated anti-rabbit secondary antibody (1:1,000, Life Technologies, catalog no. A11012) were used to reveal primary antibodies.

Morpholinos

All morpholino oligonucleotides (MOs) were purchased from Gene Tools and are listed in Table S3. MO efficiency was tested using qPCR from total RNA extracted from 10 embryos at 24 hpf. qPCR primers are listed in Table S2. *osmr*, *kita*, and *kitb* morpholinos were injected at 4 ng, 3 ng, and 8 ng, respectively, unless otherwise stated. *Kitlgb* and *osm* MOs were injected at 5 ng and 7 ng, respectively, unless otherwise stated. *Kitlgb* MO efficiency was tested using full-length primers (Table S1). *Osm* MO efficiency was tested using qPCR primers (Table S2). All MOs used in this study are splice blocking MOs.

SUPPLEMENTAL INFORMATION

Supplemental Information includes six figures, three tables, and two videos and can be found with this article online at https://doi.org/10.1016/j.stemcr.2018.04.016.

AUTHOR CONTRIBUTIONS

C.B.M. performed experiments, and C.P. provided technical support. C.B.M. and J.Y.B. designed experiments, performed analysis, and wrote the manuscript.

ACKNOWLEDGMENTS

We kindly thank Prof. David Traver for the *gata2b* ISH probe. We also thank Dr. Sylvain Lemeille for his advice on statistical analysis. J.Y.B. was endorsed by a Chair in Life Sciences funded by the Gabriella Giorgi-Cavaglieri Foundation and is also funded by the Swiss National Fund (31003A_166515) and the Fondation Privée des HUG.

Received: November 20, 2017
Revised: April 18, 2018
Accepted: April 19, 2018
Published: May 17, 2018

REFERENCES

Batsivari, A., Rybtsov, S., Souilhol, C., Binagui-Casas, A., Hills, D., Zhao, S., Travers, P., and Medvinsky, A. (2017). Understanding hematopoietic stem cell development through functional correlation of their proliferative status with the intra-aortic cluster architecture. Stem Cell Reports *8*, 1549–1562.

Bertrand, J.Y., Chi, N.C., Santoso, B., Teng, S., Stainier, D.Y., and Traver, D. (2010). Haematopoietic stem cells derive directly from aortic endothelium during development. Nature *464*, 108–111.

Bertrand, J.Y., Jalil, A., Klaine, M., Jung, S., Cumano, A., and Godin, I. (2005). Three pathways to mature macrophages in the early mouse yolk sac. Blood *106*, 3004–3011.

Bertrand, J.Y., Kim, A.D., Violette, E.P., Stachura, D.L., Cisson, J.L., and Traver, D. (2007). Definitive hematopoiesis initiates through a committed erythromyeloid progenitor in the zebrafish embryo. Development *134*, 4147–4156.

Boisset, J.C., van Cappellen, W., Andrieu-Soler, C., Galjart, N., Dzierzak, E., and Robin, C. (2010). In vivo imaging of haematopoietic cells emerging from the mouse aortic endothelium. Nature *464*, 116–120.

Cavazzana-Calvo, M., Hacein-Bey, S., de Saint Basile, G., Gross, F., Yvon, E., Nusbaum, P., Selz, F., Hue, C., Certain, S., Casanova, J.L., et al. (2000). Gene therapy of human severe combined immunodeficiency (SCID)-X1 disease. Science *288*, 669–672.

Chen, M.J., Yokomizo, T., Zeigler, B.M., Dzierzak, E., and Speck, N.A. (2009). Runx1 is required for the endothelial to haematopoietic cell transition but not thereafter. Nature *457*, 887–891.

Chi, N.C., Shaw, R.M., De Val, S., Kang, G., Jan, L.Y., Black, B.L., and Stainier, D.Y. (2008). Foxn4 directly regulates tbx2b expression and atrioventricular canal formation. Genes Dev. *22*, 734–739.

Chu, C.Y., Cheng, C.H., Chen, G.D., Chen, Y.C., Hung, C.C., Huang, K.Y., and Huang, C.J. (2007). The zebrafish erythropoietin: functional identification and biochemical characterization. FEBS Lett. *581*, 4265–4271.

Dey, G., Radhakrishnan, A., Syed, N., Thomas, J.K., Nadig, A., Srikumar, K., Mathur, P.P., Pandey, A., Lin, S.K., Raju, R., et al. (2013). Signaling network of Oncostatin M pathway. J. Cell Commun. Signal. *7*, 103–108.

Ding, L., Saunders, T.L., Enikolopov, G., and Morrison, S.J. (2012). Endothelial and perivascular cells maintain haematopoietic stem cells. Nature *481*, 457–462.

Ema, H., and Nakauchi, H. (2000). Expansion of hematopoietic stem cells in the developing liver of a mouse embryo. Blood *95*, 2284–2288.

Esashi, E., Ito, H., Minehata, K., Saito, S., Morikawa, Y., and Miyajima, A. (2009). Oncostatin M deficiency leads to thymic hypoplasia, accumulation of apoptotic thymocytes and glomerulonephritis. Eur. J. Immunol. *39*, 1664–1670.

Gao, L., Li, D., Ma, K., Zhang, W., Xu, T., Fu, C., Jing, C., Jia, X., Wu, S., Sun, X., et al. (2015). TopBP1 governs hematopoietic stem/progenitor cells survival in Zebrafish definitive hematopoiesis. PLoS Genet. *11*, e1005346.

Hess, I., and Boehm, T. (2012). Intravital imaging of thymopoiesis reveals dynamic lympho-epithelial interactions. Immunity *36*, 298–309.

Hultman, K.A., Bahary, N., Zon, L.I., and Johnson, S.L. (2007). Gene duplication of the zebrafish kit ligand and partitioning of melanocyte development functions to kit ligand a. PLoS Genet. *3*, e17.

Jin, S.W., Beis, D., Mitchell, T., Chen, J.N., and Stainier, D.Y. (2005). Cellular and molecular analyses of vascular tube and lumen formation in zebrafish. Development *132*, 5199–5209.

Khan, J.A., Mendelson, A., Kunisaki, Y., Birbrair, A., Kou, Y., Arnal-Estape, A., Pinho, S., Ciero, P., Nakahara, F., Ma'ayan, A., et al. (2016). Fetal liver hematopoietic stem cell niches associate with portal vessels. Science *351*, 176–180.

Kinoshita, T., Nagata, K., Sorimachi, N., Karasuyama, H., Sekiguchi, T., and Miyajima, A. (2001). Oncostatin M suppresses generation of lymphoid progenitors in fetal liver by inhibiting the hepatic microenvironment. Exp. Hematol. *29*, 1091–1097.

Kissa, K., and Herbomel, P. (2010). Blood stem cells emerge from aortic endothelium by a novel type of cell transition. Nature *464*, 112–115.

Mahony, C.B., Fish, R.J., Pasche, C., and Bertrand, J.Y. (2016). tfec controls the hematopoietic stem cell vascular niche during zebrafish embryogenesis. Blood *128*, 1336–1345.

Mellgren, E.M., and Johnson, S.L. (2005). kitb, a second zebrafish ortholog of mouse Kit. Dev. Genes Evol. *215*, 470–477.

Mukouyama, Y., Hara, T., Xu, M., Tamura, K., Donovan, P.J., Kim, H., Kogo, H., Tsuji, K., Nakahata, T., and Miyajima, A. (1998). In vitro expansion of murine multipotential hematopoietic progenitors from the embryonic aorta-gonad-mesonephros region. Immunity *8*, 105–114.

Murayama, E., Kissa, K., Zapata, A., Mordelet, E., Briolat, V., Lin, H.F., Handin, R.I., and Herbomel, P. (2006). Tracing hematopoietic precursor migration to successive hematopoietic organs during zebrafish development. Immunity *25*, 963–975.

Ng, E.S., Azzola, L., Bruveris, F.F., Calvanese, V., Phipson, B., Vlahos, K., Hirst, C., Jokubaitis, V.J., Yu, Q.C., Maksimovic, J., et al. (2016). Differentiation of human embryonic stem cells to HOXA+ hemogenic vasculature that resembles the aorta-gonad-mesonephros. Nat. Biotechnol. *34*, 1168–1179.

Nishikawa, M., Tahara, T., Hinohara, A., Miyajima, A., Nakahata, T., and Shimosaka, A. (2001). Role of the microenvironment of the embryonic aorta-gonad-mesonephros region in hematopoiesis. Ann. N Y Acad. Sci. *938*, 109–116.

North, T.E., Goessling, W., Walkley, C.R., Lengerke, C., Kopani, K.R., Lord, A.M., Weber, G.J., Bowman, T.V., Jang, I.H., Grosser, T., et al. (2007). Prostaglandin E2 regulates vertebrate haematopoietic stem cell homeostasis. Nature *447*, 1007–1011.

Oostendorp, R.A., Gilfillan, S., Parmar, A., Schiemann, M., Marz, S., Niemeyer, M., Schill, S., Hammerschmid, E., Jacobs, V.R., Peschel, C., et al. (2008). Oncostatin M-mediated regulation of KIT-ligand-induced extracellular signal-regulated kinase signaling maintains hematopoietic repopulating activity of Lin-CD34+CD133+ cord blood cells. Stem Cells *26*, 2164–2172.

Page, D.M., Wittamer, V., Bertrand, J.Y., Lewis, K.L., Pratt, D.N., Delgado, N., Schale, S.E., McGue, C., Jacobsen, B.H., Doty, A., et al. (2013). An evolutionarily conserved program of B-cell development and activation in zebrafish. Blood *122*, e1–e11.

Parichy, D.M., Rawls, J.F., Pratt, S.J., Whitfield, T.T., and Johnson, S.L. (1999). Zebrafish sparse corresponds to an orthologue of c-kit and is required for the morphogenesis of a subpopulation of melanocytes, but is not essential for hematopoiesis or primordial germ cell development. Development *126*, 3425–3436.

Petzer, A.L., Zandstra, P.W., Piret, J.M., and Eaves, C.J. (1996). Differential cytokine effects on primitive (CD34+CD38-) human hematopoietic cells: novel responses to Flt3-ligand and thrombopoietin. J. Exp. Med. *183*, 2551–2558.

Ribeil, J.A., Hacein-Bey-Abina, S., Payen, E., Magnani, A., Semeraro, M., Magrin, E., Caccavelli, L., Neven, B., Bourget, P., El Nemer, W., et al. (2017). Gene therapy in a patient with sickle cell disease. N. Engl. J. Med. *376*, 848–855.

Rose, T.M., Weiford, D.M., Gunderson, N.L., and Bruce, A.G. (1994). Oncostatin M (OSM) inhibits the differentiation of pluripotent embryonic stem cells in vitro. Cytokine *6*, 48–54.

Rybtsov, S., Batsivari, A., Bilotkach, K., Paruzina, D., Senserrich, J., Nerushev, O., and Medvinsky, A. (2014). Tracing the origin of the HSC hierarchy reveals an SCF-dependent, IL-3-independent CD43(-) embryonic precursor. Stem Cell Reports *3*, 489–501.

Sato, F., Miyaoka, Y., Miyajima, A., and Tanaka, M. (2014). Oncostatin M maintains the hematopoietic microenvironment in the bone marrow by modulating adipogenesis and osteogenesis. PLoS One *9*, e116209.

Tamplin, O.J., Durand, E.M., Carr, L.A., Childs, S.J., Hagedorn, E.J., Li, P., Yzaguirre, A.D., Speck, N.A., and Zon, L.I. (2015). Hematopoietic stem cell arrival triggers dynamic remodeling of the perivascular niche. Cell *160*, 241–252.

Tamura, S., Morikawa, Y., Miyajima, A., and Senba, E. (2002). Expression of oncostatin M in hematopoietic organs. Dev. Dyn. *225*, 327–331.

Tanaka, M., Hirabayashi, Y., Sekiguchi, T., Inoue, T., Katsuki, M., and Miyajima, A. (2003). Targeted disruption of oncostatin M receptor results in altered hematopoiesis. Blood *102*, 3154–3162.

Tanaka, M., and Miyajima, A. (2003). Oncostatin M, a multifunctional cytokine. Rev. Physiol. Biochem. Pharmacol. *149*, 39–52.

Thisse, C., Thisse, B., Schilling, T.F., and Postlethwait, J.H. (1993). Structure of the zebrafish snail1 gene and its expression in wild-type, spadetail and no tail mutant embryos. Development *119*, 1203–1215.

Tian, Y., Xu, J., Feng, S., He, S., Zhao, S., Zhu, L., Jin, W., Dai, Y., Luo, L., Qu, J.Y., et al. (2017). The first wave of T lymphopoiesis in zebrafish arises from aorta endothelium independent of hematopoietic stem cells. J. Exp. Med. *214*, 3347–3360.

Traver, D., Paw, B.H., Poss, K.D., Penberthy, W.T., Lin, S., and Zon, L.I. (2003). Transplantation and in vivo imaging of multilineage engraftment in zebrafish bloodless mutants. Nat. Immunol. *4*, 1238–1246.

Wallace, P.M., MacMaster, J.F., Rillema, J.R., Peng, J., Burstein, S.A., and Shoyab, M. (1995). Thrombocytopoietic properties of oncostatin M. Blood *86*, 1310–1315.

Wang, S., He, Q., Ma, D., Xue, Y., and Liu, F. (2015). Irf4 regulates the choice between T lymphoid-primed progenitor and myeloid lineage fates during embryogenesis. Dev. Cell *34*, 621–631.

Westerfield, M. (1994). The Zebrafish Book: A Guide for the Laboratory Use of Zebrafish (*Brachydanio rerio*) (University of Oregon Press).

Zhu, H., Traver, D., Davidson, A.J., Dibiase, A., Thisse, C., Thisse, B., Nimer, S., and Zon, L.I. (2005). Regulation of the lmo2 promoter during hematopoietic and vascular development in zebrafish. Dev. Biol. *281*, 256–269.

Zovein, A.C., Hofmann, J.J., Lynch, M., French, W.J., Turlo, K.A., Yang, Y., Becker, M.S., Zanetta, L., Dejana, E., Gasson, J.C., et al. (2008). Fate tracing reveals the endothelial origin of hematopoietic stem cells. Cell Stem Cell *3*, 625–636.